W-deposited contacts with carbon nanofiber using focused ion and electron beams

Shusaku Maeda[1], Toshishige Yamada[1], Patrick Whilhite[1], Hisashi Yabutani[2], Tsutomu Saito[2], and Cary Y. Yang[1]
[1]Santa Clara University, Center for Nanostructures
500 El Camino Real, Santa Clara, California 95053, USA
[2]Hitachi High-Technologies Corporation,
882 Ichige, Hitachinaka, Ibaraki 312-8504, Japan
Email: smaeda@scu.edu

***Abstract*—Carbon nanofiber (CNF) is promising as a next-generation on-chip interconnect material. Understanding the temperature dependence of CNF resistance is important in evaluating its potential for such interconnect applications. In a CNF test device, contacts formed by tungsten (W) deposition using focused ion beam (FIB) is effective in minimizing the effect of unwanted parasitics, thus yielding a more accurate determination of the temperature dependence. However, FIB deposition can potentially damage devices because of its high energy. We propose to use a gas-injection system for low-energy electron-beam deposition with fine precision in a variable-pressure scanning electron microscope. The results of W-deposited CNF devices obtained using electron beam (e-beam) are compared with their FIB counterparts.**

Index Terms – Carbon nanofiber, electrothermal transport, FIB, e-beam-induced deposition.

I. INTRODUCTION

CNF is a promising material for interconnect applications in next-generation silicon integrated circuits because of its demonstrated high current capacity and excellent mechanical and thermal properties. Since the temperature dependence of its material properties such as conductivity relates directly to circuit performance, an in-depth understanding is critically important. However, in practice, it is extremely difficult to monitor and control the temperature of the test device and maintain thermal equilibrium because of its small thermal capacity. To circumvent this problem, we examine the increase in temperature due to Joule heating of a current-stressed device and deduce the temperature from the stress current using a heat transport model previously developed by our group [1]. Thus the measured conductivity can then be obtained as a function of temperature.

Each test device is prepared by first drop-casting a single CNF between a pair of patterned gold (Au) electrodes on a SiO_2 substrate. The contacts are then formed using FIB to deposit W directly onto the CNF-drop-casted Au electrodes [2]. The resulting resistance is smaller than that for the pre-W-deposited device by a factor of 10^3 or more. Therefore, contact formation by depositing W or other metals is vital to minimizing contact resistance and improving device and circuit performance. In general, W-deposition by FIB is an efficient and effective process, but its high energy can potentially damage the devices. Therefore, we develop an alternative technique for metal deposition using a well-controlled electron beam in a variable-pressure scanning electron microscope (VP-SEM). In this configuration, the precursor gas is delivered via a specially designed gas-injection system (GIS) and guided by the focused electron beam to yield deposition on a selected target at low energy [3]. The technique is more cost-effective as the GIS can be one of the modules in an existing SEM, which allows for *in situ* imaging and elemental analysis before, during, and after deposition. In this study, we compare the resistances of CNF test devices formed with W-deposition using FIB and e-beam deposition techniques. Such a comparison will lead to improvements in our e-beam deposition system and better control of properties of contacts between metal and CNF.

II. FIB W-DEPOSITED CNF DEVICES

CNFs in this study were grown using plasma-enhanced chemical vapor deposition technique with Ni catalyst [4]. These CNFs were drop-casted onto a SiO_2 substrate of patterned Au electrodes after dispersing in isopropyl alcohol. The horizontal CNF test device can be used as a prototype of interconnect lines between adjacent transistors in the same silicon layer. These fabricated test devices then underwent W deposition at the electrodes using FIB to improve the contact resistance. Figure 1 shows an SEM image of the resulting test device [2].

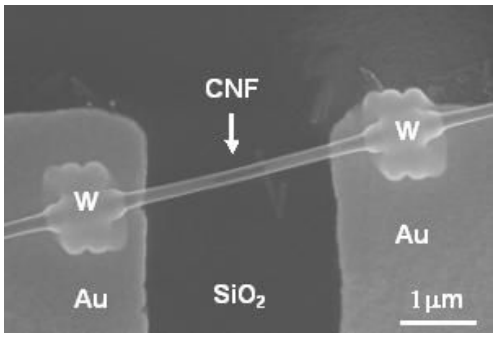

Figure 1. SEM image of CNF drop-casted between Au electrodes, with FIB-deposited W electrode contacts.

In our previous study, we compared the resistances of CNF test devices on Au electrodes with and without W deposition [2]. The measured contact resistance between CNF and Au electrodes was significantly reduced by W-deposition, from MΩ to kΩ range [2].

In order to examine the CNF resistance at higher temperatures, stressing current was applied to FIB W-deposited test devices in progression, i.e., in the initial cycle, a small current was applied for three minutes, and in the next and subsequent cycles, a larger current was applied for another three minutes each after the test device was cooled down to ambient temperature. We measured the average resistance during each stress cycle and related it to the stressing current. The stressing current generated Joule heat which can be converted into temperature using a heat transport model reported previously [1]. The conductivity of each of four test devices increases monotonically with temperature, as shown in Fig. 2.

In general, the conductivity of metals decreases with increasing temperature due to increasing phonon scattering [5]. Our CNF, although exhibiting linear current-voltage characteristics [6], shows the opposite trend, with conductivity increasing with increasing temperature. We attribute this to defects in the nanofiber that serve as electron traps, with detrapping of electron due to Joule heating [5,7-8]. Figure 2 shows an Arrhenius plot of the conductivity versus reciprocal temperature, revealing a thermal activation process characterized by an activation energy. The extracted activation energy values (22~35 meV) are consistent with that (26 meV) obtained in a previous study for vertically aligned CNF via structures [7].

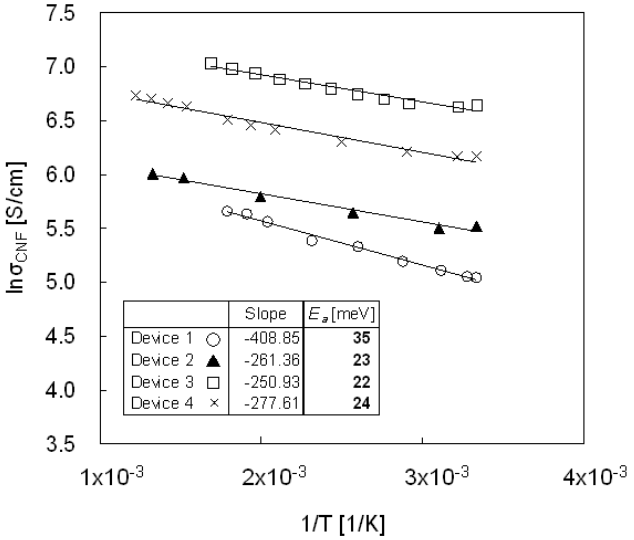

Figure 2. CNF conductivity σ_{CNF} as a function of inverse temperature $1/T$ and activation energies for four devices with FIB-deposited W electrode contacts.

III. E-BEAM INDUCED DEPOSITION OF TUNGSTEN

As described in Sec. II, the study of CNF devices with FIB-deposited W electrode contacts yielded important new findings. In view of the current continuous downward scaling trend, metal deposition requires more sophisticated control and finer resolution, as well as better cost-effectiveness than what FIB can offer. In addition, FIB has the potential risk for damages to the devices because of its high energy. Furthermore, there is also a concern about sample contamination by gallium (Ga) as the ion source because of its semiconducting property. To address these issues, we develop an e-beam deposition technique using a GIS with high precision in controlling gas flow and low beam energy. Deposition by ion beam requires a dual system (FIB and SEM), while e-beam deposition requires only an SEM with a GIS module. The GIS consists of a narrow nozzle, a pressure gauge, two needle valves, a source gas bottle and a gas injector as shown in Figure 3. The nozzle is placed at the point where deposition occurs using a manual controller. The tip of the nozzle is moved very close to the surface of the target device by adjusting the height of the SEM stage. In addition, the size of the nozzle is chosen to optimize gas flow. We use WF_6 as the precursor gas for W deposited onto the CNF-Au electrode contacts to avoid having to preheat powder precursors such as $W(CO)_6$. The precursor, WF_6, is injected via the GIS into the SEM chamber.

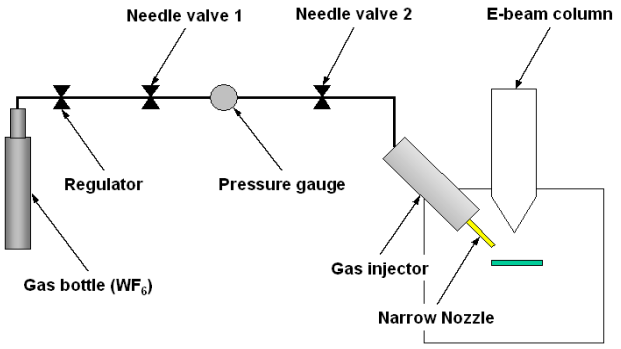

Figure 3. Schematic of the e-beam-induced deposition system including the GIS.

Comparison of the results for W-deposition by ion and electron beams is important because W is known to form excellent electrical contacts with many materials. At the same time, such a comparison affords us the opportunity to evaluate our e-beam deposition system and the effectiveness of the gas injection process. Parameters such as the SEM working distance, distance from the targeted spot to the

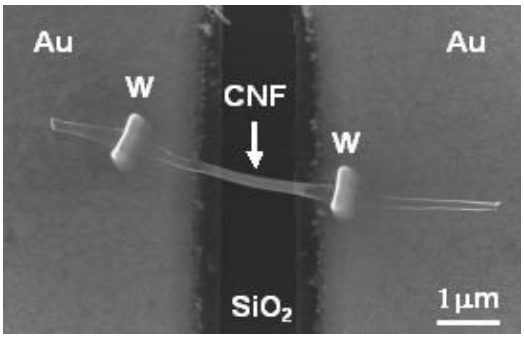

Figure 4. SEM image of CNF drop-casted between Au electrodes, with e-beam-induced deposited W electrode contacts.

nozzle tip, gas flow rate, and gas pressure are examined. Also the e-beam acceleration voltage, emission current, scan mode, and dwell time are optimized. We use a working distance of 25 mm and the distance from the targeted spot to the nozzle tip is adjusted to within 0.1 mm using a manual controller for the SEM stage. The e-beam acceleration voltage is 30 kV and the emission current is 150 μA. The beam impinges upon the targeted spot on the CNF-Au electrode for 30 minutes with the line scan as the scan mode, while WF_6 flows out of the nozzle. As a result, the dissociated W is deposited onto the targeted spot to form a W-CNF-Au electrode contact, as shown in Figure 4.

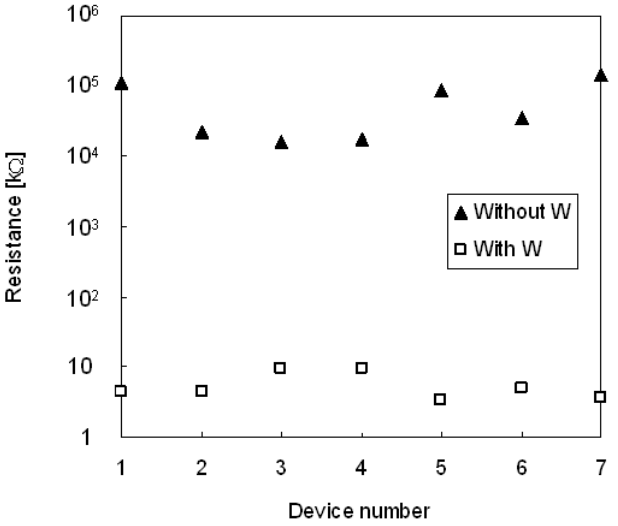

Figure 5. Comparison of resistances of CNF test devices before and after W deposition with e-beam.

We measure the current-voltage characterizations of seven CNF test devices before and after W-deposition. Figure 5 shows the measured resistances before and after W deposition. The resistances of all measured devices are decreased by more than 10^3 due to the formation of the e-beam-deposited W contacts, from MΩ to kΩ range. This improvement is comparable to that obtained using FIB [2]. The temperature dependence of resistance for these CNF test devices with e-beam-deposited W contacts will also be determined, similar to our recent study [8]. The resulting activation energy can be used as a parameter for characterizing W-deposited contacts.

ACKNOWLEDGMENT

This work was supported by the United States Army Space and Missile Defense Command (SMDC) and carries Distribution Statement A, approved for public release, distribution unlimited, and by Hitachi High Technologies America.

REFERENCES

[1] T. Yamada, T. Saito, D. Fabris, and C. Y. Yang, IEEE Elec. Dev. Lett. **30**, 469 (2009).

[2] T. Saito, T. Yamada, D. Fabris, H. Kitsuki, P. Wilhite, M. Suzuki, and C. Y. Yang, Appl. Phys. Lett., **93**, 102108 (2008).

[3] D. C. Joy and P. D. Rack, Microscopy and Microanalysis, NY, **11**, 816 (2005).

[4] B. A. Cruden, A. M. Cassell, Q. Ye, and M. Meyyappan, J. Appl. Phys. **94**, 4070 (2003).

[5] T. Ando, A. B. Fowler, and F. Stern, Rev. Mod. Phys, **54**, 437 (1982).

[6] T. Yamada, T. Saito, M. Suzuki, P. Wilhite, X. Sun, N. Akhavantafti, D. Fabris, and C. Y. Yang, J. Appl. Phys. **107**, 044304 (2010).

[7] Q. Ngo, T. Yamada, M. Suzuki, Y. Ominami, A. M. Cassell, J. Li, M. Meyyappan, and C.Y. Yang, IEEE Trans. Nanotech. **6**, 688 (2007).

[8] T. Yamada, H. Yabutani, T. Saito, and C.Y. Yang, Nanotechnology **21**, 265707 (2010).